Journal of Zhejiang University-SCIENCE A 2026 27(10):1169-1180
www.jzus.zju.edu.cn; www.springer.com/journal/11582
E-mail: jzus_a@zju.edu.cn

Research Article
https://doi.org/10.1631/jzus.A2500676

Check for updates

Mechanical degradation characterization in remolded moraine soils and microstructure evolution under freeze–thaw cycles

Tuo LU[1,2,3,4], Yongbo TIE[1,2]✉, Sai K. VANAPALLI[4], Zhaoyu LI[1,2]

[1]*Chinese Academy of Geological Sciences, Beijing 100037, China*
[2]*Chengdu Center of China Geological Survey, Chengdu 610218, China*
[3]*School of Engineering and Technology, China University of Geosciences, Beijing 100083, China*
[4]*Department of Civil Engineering, University of Ottawa, Ottawa K1N 6N5, Canada*

Abstract: Remolded moraine soils are highly susceptible to degradation caused by freeze–thaw (F-T) cycles, posing significant risks to the stability of slopes in hilly regions. This study investigates the mechanical degradation and microstructural changes induced by F-T cycles through a comprehensive experimental program, including F-T cycle tests, triaxial shear tests, unconfined compression tests, and micro-computed tomography (micro-CT) scanning of moraine soil from the southeast of the Xizang Autonomous Region, China. The results reveal three stages of mechanical parameter degradation: rapid decline, moderate reduction, and plateau. Cohesion, initial average elastic modulus, and strength decrease significantly under low confining pressure (40%–50% reduction), while the decrease is less pronounced under higher pressures (10%–30%). Micro-CT scanning shows a clear evolution in the microstructure, with the porosity increasing from 14.25% to 18.69% and the pore-crack size rising from 69.83 to 90.44 μm. These microstructural changes are identified as the primary mechanism behind macroscopic degradation. A new gray model was developed to predict mechanical parameter evolution, showing high accuracy for predicting the strength of moraine soils in later F-T cycles (e.g., 15th, 20th, and beyond). The new gray model provides valuable insights for the design of moraine slopes and infrastructure subjected to F-T conditions.

Key words: Moraine soils; Freeze–thaw (F-T) cycles; Mechanical degradation; Micro-computed tomography (micro-CT); Gray models

1 Introduction

With the advancement of key national strategies such as China's Western Development, the Belt and Road Initiative, and the ongoing development of critical railways and highways, addressing the challenges posed by frost damage in cold regions has become increasingly crucial (Li et al., 2022; Zeng et al., 2024). Freeze–thaw (F-T) cycles in high-altitude mountainous areas are a significant factor both with respect to engineering safety and soil erosion processes in moraine soils (Wu et al., 2010; Wang et al., 2025).

Moraine soils, formed by the deposition and transport of sediments by glaciers, are widely distributed in the Xizang Autonomous Region of China. These soils are primarily sandy or gravelly, with significant proportions of silt and clay content (Jiang et al., 2020; Li et al., 2022; Lu et al., 2025).

Over the past decades, numerous geohazards involving moraine soils that include landslides, glacial lake outburst floods, and glacial debris flows are partly attributed to the influence of repeated F-T cycles in various regions of the world, including Alaska, Greenland, northern Canada, Russia, and Xizang, China (Emmer et al., 2020; Rechberger et al., 2021; Allen et al., 2022; Wang et al., 2024). Most of these geohazards arise due to the degradation of the mechanical properties of moraine soils and glacial tills (Cui et al., 2013; Chen et al., 2019). In recent years, some researchers have focused on the mechanical behavior of remolded moraine soils. Some studies have shown that the shear strength of moraine soils significantly decreases with increasing degree of saturation or water content (Winter, 2004; Han et al., 2016; Vanapalli and

✉ Yongbo TIE, tyongbo@mail.cgs.gov.cn
Yongbo TIE, https://orcid.org/0000-0001-7241-2942
Tuo LU, https://orcid.org/0000-0001-6019-188X
Sai K. VANAPALLI, https://orcid.org/0000-0002-3273-6149

Received Dec. 31, 2025; Revision accepted May 28, 2026;
Crosschecked June 24, 2026; Online first July 24, 2026

© Zhejiang University Press 2026

Han, 2016; Zhou et al., 2019). Several studies have investigated remolded moraine soils with a relative density greater than 70%, which exhibit significantly higher shear strength (Jiang Y et al., 2024; Zeng et al., 2024). Some studies suggest that uniaxial compressive and triaxial shear strength decrease substantially with increasing F-T cycles, with cohesion showing an exponential decline (Chen et al., 2024; Fan et al., 2024; Jiang TT et al., 2024). Additionally, Li et al. (2025) conducted numerical simulations to assess mechanical damage in remolded moraine soils subjected to F-T cycles using the discrete element method (DEM). However, there is a lack of mathematical equations describing the degradation of mechanical parameters in remolded moraine soils under F-T cycles. Furthermore, the evolution of the 3D pore-crack structure in moraine soils under F-T cycles was hardly revealed.

Several researchers in recent years have used X-ray computed tomography (CT), known for its nondestructive nature and high resolution, to characterize the 3D microstructural features of soils (Yu et al., 2024). Hence, X-ray CT can be a valuable tool for quantifying the development of pores and cracks during F-T cycles, offering new insights into the micromechanisms that drive strength deterioration in remolded moraine soils.

This study explores the mechanical deterioration of remolded moraine soils subjected to F-T cycles through triaxial shear tests (TSTs) and unconfined compression tests (UCTs). X-ray CT and deep learning technology were employed to characterize the microstructure and evolution of pore cracks during F-T cycles. Furthermore, a new gray model was developed to fit and predict the key mechanical strength parameters of moraine soils (e.g., shear strength, cohesion, and initial average elastic modulus) under F-T cycles.

2 Materials and methods

2.1 Investigation and sampling

This study site (longitude: 94.74557584°E, latitude: 29.48186613°N, World Geodetic System 1984 (WGS-84)) is located along the lower Yarlung Tsangpo River in southeastern Xizang and is characterized by a monsoon maritime climate, with precipitation primarily concentrated in summer. It is characterized by marine-type glaciers influenced by moist airflows from the Indian Ocean, which can be classified as a seasonally frozen terrain. Moraine soils and glacial tills are widely distributed in the southeastern Xizang, with a notable concentration extending from Bomi County to Milin City in Nyingchi City (Li et al., 2022).

Fig. 1 illustrates the details of the glacial and moraine surface survey, as well as some tests conducted in this study. Moraine soil was collected from Danniang Township, Milin City (at an altitude of 2970 m above sea level).

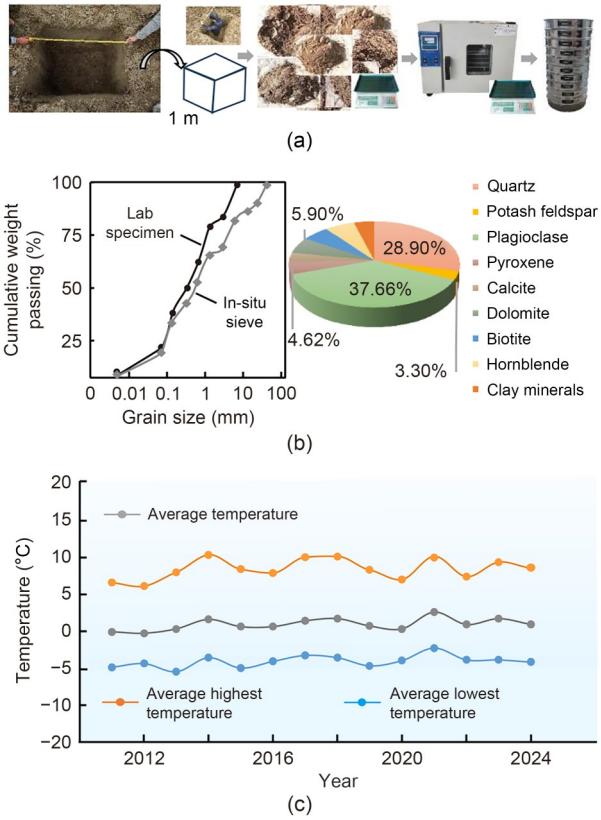


Fig. 1 Study area and sampling: (a) representative soil sample collection from a test pit of 1 m depth for performing various tests; (b) grain size analysis results and mineral composition; (c) January information of temperature in Milin City (http://data.cma.cn/)

Figs. 1a and 1b show the sieve analysis equipment and the grain size distribution (GSD) results, respectively. The GSD reveals a composition of 10.35% fine grains (<0.075 mm), 51.87% sand (0.075–2 mm), and 37.78% gravel (2–60 mm). X-ray diffraction (XRD) was employed to identify the mineral components in the soil; the major minerals identified included quartz, plagioclase, hornblende, dolomite, calcite, and various clay minerals (Fig. 1b). Notably, quartz and plagioclase

constitute significant proportions of this mineral assemblage, at approximately 28.90% and 37.66%, respectively.

The moraine soil in the study area is classified as unconsolidated and exhibits a loose structure. Due to the lack of cementation, collecting undisturbed field samples is challenging, as the soil crumbles easily with minimal disturbance. The similarity ratio method is often employed to prepare remolded samples, where the soil is remixed and compacted to match the engineering properties of undisturbed soils as closely as possible (Feng et al., 2008). To address this, in this study, a remolded sample approach is extended for preparing specimens with comparable characteristics to overcome the lack of natural cementation and ensure consistency in sample structure for subsequent analysis.

2.2 F-T cycles and mechanical tests

Table 1 presents the basic physical properties of the moraine soils. The moisture content of in-situ moraine soils varies from 2.20% to 9.69%. The plastic and liquid limits are 15.1% and 21.6%, respectively. The dry density (ρ_d) is approximately 1.9–2.0 g/cm^3. The specific gravity (G_s) is 2.66.

Table 1 Physical properties of remolded moraine soils

G_s	ρ_d (g/cm^3)	e	ω_0 (%)	Filed grain size scale (mm)	Grain size scale in test (mm)
2.66	1.9	0.4	10	0.001–60	0.001–10

e: void ratio; ω_0: moisture content in test

The initial moisture content of the remolded moraine soil specimens was controlled during specimen preparation (Fig. 2a). First, a predetermined mass of oven-dried particles was weighed (removing ⩾10 mm particles because the maximum particle size should be smaller than 1/6–1/10 the diameter of the specimen, GB/T 50123-2019 (MOHURD and SAMR, 2019)), and the required amount of deionized water was calculated according to the target moisture content. Both the in-situ gradation curve and the lab gradation curve after particle removal are shown in Fig. 1b. Deionized water was gradually sprayed onto the soil using a fine-mist sprayer while the soil was continuously mixed to promote uniform water distribution. During this process, the wetted soil mass was repeatedly weighed to ensure that the target moisture content was achieved. After that, the compaction process was carried out in five equal layers, with each layer carefully placed and compacted to ensure uniform density distribution throughout the specimen height (cylindrical specimens: 61.8 mm in diameter and 125.0 mm in height). The wetted specimen soil was sealed and stored for 24 h to allow moisture equilibration. In addition, specimens with a gravel fraction (>2 mm) less than 40% by mass were tested using a conventional triaxial or direct shear apparatus to measure mechanical properties (MOHURD and SAMR, 2019).

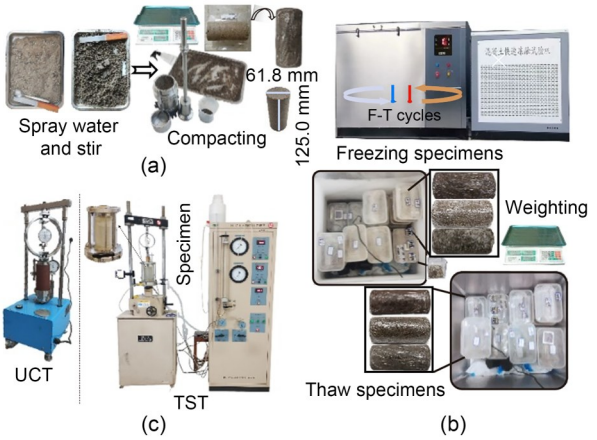


Fig. 2 F-T cycles and mechanical tests: (a) remolded specimen preparation; (b) F-T cycles; (c) UCT and TST

During the F-T cycle tests, each compacted specimen was tightly wrapped with plastic film and then placed in a small box and sealed. This combined sealing method was used to minimize moisture exchange between the specimen and the external environment. The specimens were weighed before and after F-T cycles to check possible moisture variation. The weighing results indicated that moisture loss during F-T cycling was very limited. Therefore, no additional water was supplied during the F-T process, and the tests were conducted under sealed, relatively closed moisture conditions.

Over the past decades, January has been the coldest month in this region's winter conditions, characterized by semiarid conditions with minimal precipitation and an average temperature of 0.9 ℃. The average lowest temperature in January ranges from −2.3 to −5.5 ℃ (Fig. 1c), while the average highest temperature ranges from 6.1 to 9.6 ℃. Nighttime durations generally exceed 12 h, while daytime durations are shorter. Consequently, the freezing temperature and duration were set at −6.0 ℃ and 13 h, respectively, in

this study. At this temperature, −6 °C is sufficient to freeze the pore water within moraine soils (Wei et al., 2025). Subsequently, thawing was conducted at 10.0 °C for 11 h. This entire process was considered one F-T cycle (Fig. 2b). Several studies suggest that most degradation of mechanical properties occurs within the first 20 F-T cycles (Fan et al., 2024; Jiang TT et al., 2024; Qiu et al., 2024). Hence, zero, two, five, 10, 15, and 20 cycles were applied to the specimens in a temperature-controlled F-T device (error ±0.5 °C).

As shown in Fig. 2c, the specimens' mechanical properties were measured via UCTs (loading rate is 1.0 mm/min; maximum axial force capacity is 7.5 kN) and conventional unconsolidated undrained (UU) TSTs (loading rate is 0.8 mm/min; maximum axial force capacity is 100 kN).

2.3 Micro-computed tomography scanning

For the micro-computed tomography (micro-CT) scanning tests, irregular sub-specimens (SS1, SS2, and SS3) were carefully selected from the central part of the corresponding large cylindrical specimens without F-T cycles (Fig. 3a1). SS3 was applied in the mercury intrusion porosimetry (MIP) test (Micro Active AutoPore V9600 device equipped with a large-volume dilatometer (Micromeritics Instrument Corporation, USA)). The MIP results revealed the pore size distribution across a broader range, including the micropores, which were less well captured by micro-CT.

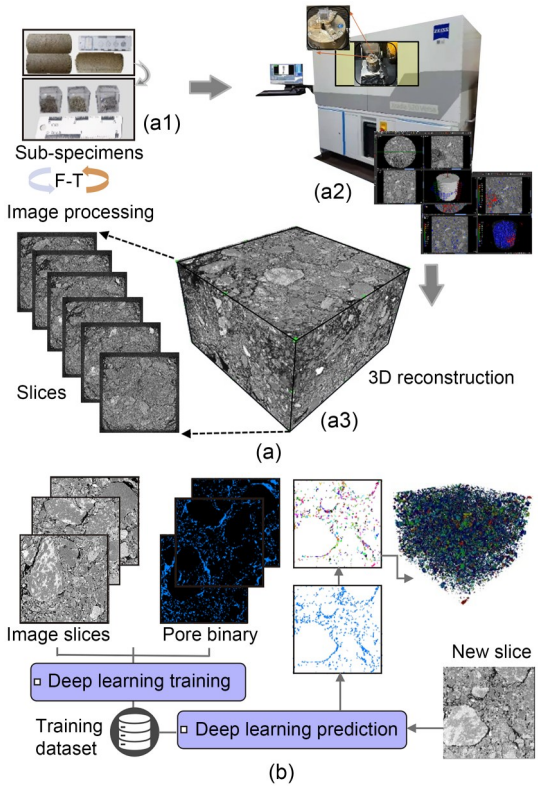


Fig. 3 Micro-CT scanning and image procedure: (a) CT scanning; (b) deep learning segmentation of pore cracks

This selection strategy was adopted to reduce possible boundary effects caused by specimen preparation and surface disturbance. The selected sub-specimens had no visible cracks or artificial damage caused by cutting or handling, and had comparable sizes suitable for micro-CT scanning. Therefore, although the micro-CT specimens were irregular in shape, they were considered representative of the internal microstructural characteristics of the corresponding F-T cycle specimens. To improve the comparability of the micro-CT results, all selected specimens were scanned under the same scanning parameters, and the reconstructed images were processed using the same region-of-interest selection, deep learning model, and pore-structure analysis procedure. Three irregular sub-specimens were prepared for micro-CT scanning by placing them in a container with approximate dimensions of 15 mm×15 mm×15 mm (Figs. 3a and 3b).

Micro-CT scanning was performed using the Xradia 520 Versa system manufactured by Zeiss, Germany. The scanning resolution was 8.0 μm per pixel, with a maximum scanning volume of 10 mm in width and height. Each scan produced approximately 1200 slice images of raw data (1700 pixels×1700 pixels per slice, 16-bit grayscale). The operating voltage and current were set to 50 kV and 81 μA, respectively (Fig. 3a2). The initial micro-CT images were first preprocessed to enhance image quality and prepare them for subsequent analysis. A nonlocal means filter was applied to suppress noise while preserving edge details. The filtered images were then cropped to a uniform resolution of 1024 pixels×1024 pixels×800 slices, and the grayscale range was normalized to [0, 255], ensuring consistent data dimensions across all sub-specimens (Fig. 3a3).

To identify and quantify pore-crack and grain structures in remolded moraine soils, an enhanced U-Net convolutional neural network was employed (Alom et al., 2019; Minaee et al., 2022). The U-Net model performs pixel-level semantic segmentation of CT images by learning multiscale features of fractures through deep convolutional and deconvolutional layers. This

deep learning-based segmentation was implemented in MATLAB or AVIZO, leveraging the platforms' capabilities for deep learning model development and visualization of 3D structures. MATLAB was used to train and test the network, and AVIZO was used for 3D image processing and feature visualization. The micro-CT image dataset comprises 12000 CT images, divided into a test set (8000 images) and a training set (4000 images) (Fig. 3b). The training images have a resolution of 1024 pixels×1024 pixels. They are specifically designed to focus on the analysis of pore cracks. When using the U-Net network algorithm for training (Liu et al., 2024), the batch size is set to 64, the epoch is set to 1000, and the learning rate is set to 0.0001.

Based on the separation results, several microstructural parameters were extracted from 3D CT images to describe the geometric characteristics of pore-crack networks, including the porosity, pore size, and fractal dimension (Wei et al., 2020; Lu et al., 2023; Liu et al., 2024).

(1) The 3D porosity is the ratio of pore-crack voxels to the total number of voxels within the analyzed volume.

(2) The equivalent pore width (W_{EqW}) is defined based on the volume of the pore or crack and is calculated as follows:

$$W_{\mathrm{EqW}}=\sqrt{\frac{4V}{\pi L}}, \tag{1}$$

where L is the longest Feret diameter of the pore-crack; V is the pore-crack volume.

(3) The fractal dimension (D_{v}) is calculated as follows:

$$D_{\mathrm{v}}=\frac{\ln\delta}{\ln(N(\delta))}, \tag{2}$$

where δ represents the size of the measuring voxel box; $N(\delta)$ is the number of boxes of size δ required to cover the connected pore cracks.

3 New gray model

Several key mechanical parameters, including strength (q) (triaxial shear strength (q_{t}) and unconfined compression strength (q_{u})), initial average elastic modulus (E_0), and cohesion (c), were selected to evaluate the mechanical degradation behavior of remolded moraine soils under F-T cycles (Fig. 4a). In addition, the F-T cycle deterioration rates, K_1–K_3, for the deterioration of moraine soil mechanics are summarized below:

$$\begin{cases} K_1=1-\dfrac{E_0(N)}{E_0(0)}, \\ K_2=1-\dfrac{q(N)}{q(0)}, \\ K_3=1-\dfrac{c(N)}{c(0)}, \end{cases} \tag{3}$$

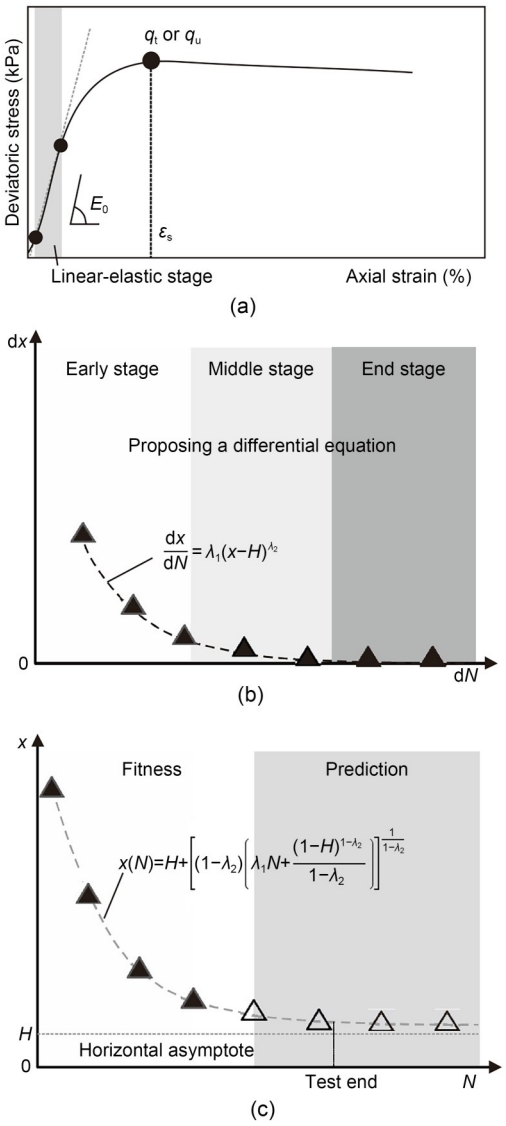


Fig. 4 New gray model: (a) mechanical parameters; (b) gray differential equation; (c) solution of the differential equation. The parameters are explained in the text

where $E_0(0)$, $q(0)$, and $c(0)$ are the zero F-T cycle initial elastic modulus, strength, and cohesion, respectively. $E_0(N)$, $q(N)$, and $c(N)$ are the N-cycle values. The parameters K_1^* and K_2^* are the experimentally measured maximum deterioration rates K_1 and K_2, respectively.

The mechanical degradation behavior of soils subjected to F-T cycles generally exhibits a nonlinear trend, which can be categorized into three distinct stages (Fig. 4b): an early stage with rapid strength loss, a middle stage with a decelerated degradation rate, and the end stage where the strength tends to stabilize and no longer change significantly (Chen et al., 2024; Fan et al., 2024; Jiang TT et al., 2024; Qiu et al., 2024).

A gray differential model (Eq. (4)) is proposed to capture the degradation pattern of remolded moraine soils. This model allows the formulation of a differential equation where the degradation rate of mechanical parameters is expressed as a function of the number of F-T cycles. The observed mechanical parameters after N F-T cycles are denoted as a time series: $x=\{x(0), x(1), \cdots, x(N)\}$, where x represents the initial average elastic modulus (E_0), strength (q_t or q_u), or cohesion (c). The first-order difference Δx is obtained by subtracting adjacent values in the sequence.

$$\Delta x=\{x(1)-x(0), x(2)-x(1), \cdots, x(N)-x(N-1)\}\approx \mathrm{d}x. \tag{4}$$

A nonlinear gray differential model is then assumed in the form of:

$$\begin{cases} x=\dfrac{\mathrm{d}x}{\mathrm{d}N}=\lambda_1(x-H)^{\lambda_2}, \quad \lambda_1<0,\ \lambda_2>1, \\ H=(1-K^*)\cdot x(0), \end{cases} \tag{5}$$

where $\mathrm{d}x/\mathrm{d}N$ denotes the change rate, λ_1 and λ_2 are autofitting parameters, and H is a horizontal asymptote representing the deterioration limit for estimating the ultimate value of strength after long F-T cycles. The parameter H can be calculated based on the F-T cycle deterioration rates K_1 and K_2. The parameter K^* is the empirical or experimentally measured maximum deterioration rate K_1^* or K_2^*, according to K_1 or K_2 (Eq. (3)).

Taking the limits of Eq. (5) under the conditions $x\to H$ and $x>H$, the following expressions can be obtained:

$$\begin{cases} \lim\limits_{\substack{N\to+\infty \\ x\to H}}\left(\lambda_1(x-H)^{\lambda_2}\right)=0, \\ \lim\limits_{\substack{N\to 0^+ \\ x>H}}\left(\lambda_1(x-H)^{\lambda_2}\right)=\lambda_1[x(0)-H]^{\lambda_2}. \end{cases} \tag{6}$$

This implies that as x approaches H and N approaches $+\infty$, the rate of change asymptotically tends to zero, indicating stabilization in the degradation process (Fig. 4b).

Next, this study solves Eq. (5):

$$\int \frac{1}{(x-H)^{\lambda_2}}\mathrm{d}x=\int \lambda_1 \mathrm{d}N, \tag{7}$$

$$x(N)=H+[(1-\lambda_2)(\lambda_1 N+C)]^{\frac{1}{1-\lambda_2}}. \tag{8}$$

Substitute $x(0)$ into Eq. (8) to calculate the integration constant C and $x(N)$.

$$C=\frac{(x(0)-H)^{1-\lambda_2}}{1-\lambda_2}, \tag{9}$$

$$\begin{cases} x(N)=H+\left[(1-\lambda_2)\left(\lambda_1 N+\dfrac{(1-H)^{1-\lambda_2}}{1-\lambda_2}\right)\right]^{\frac{1}{1-\lambda_2}}, \\ H=(1-K^*)\cdot x(0), \quad \lambda_1>0,\ \lambda_2<1. \end{cases} \tag{10}$$

Eqs. (5) and (10) are also named the new gray models and the MATLAB code can be found at https://github.com/LuTuo123/LGM.

The new model parameters λ_1 and λ_2 were estimated via nonlinear least squares fitting using the lsqcurvefit function. The model remains applicable even when limited information on mechanical properties is available. This technique provides a robust and data-efficient framework for predicting the mechanical parameters of moraine soils for 10–20 F-T cycles using limited information from zero to 10 F-T cycles.

Taking the limit as $N\to+\infty$:

$$\lim_{\substack{N\to+\infty \\ x\to H}} x(N)=H+\lim_{N\to+\infty}\left(\left[(1-\lambda_2)\left(\lambda_1 N+\frac{(1-H)^{1-\lambda_2}}{1-\lambda_2}\right)\right]^{\frac{1}{1-\lambda_2}}\right)= H+\frac{1}{(+\infty)^{\lambda_2-1}}=H. \tag{11}$$

4 Results and discussion

4.1 Stress–strain curves

In typical strain-softening behavior, specimens exhibit an obvious peak followed by a significant reduction in stress resistance as the soil is strained. The stress–strain curve remains stable and gradually decreases with increasing strain after the yield strain (ε_s) (Fig. 5). The q_u and q_t decrease with the F-T cycles, and the difference Model the peak shear strength (q_u and q_t) and resident strength decreases. After 20 F-T cycles, the narrowest gap between the peak shear strength (q_t) and residual strength is attributed to the progressive degradation of the soil structure and the development of pore-crack networks, particularly under a confining pressure (σ_3) of 200 kPa.

4.2 Mechanical deterioration under F-T cycles

In the UCT, the specimen's initial average elastic modulus (E_0) decreased from 3.20 to 1.50 MPa as the number of F-T cycles increased from 0 to 20. The strength (q_u) of the specimen decreased from 40.80 to 24.08 kPa as the number of F-T cycles rose from 0 to 20. Under different confining pressures (σ_3), both the initial average elastic modulus (E_0) and the shear strength (q_t) showed a decreasing trend with increasing F-T cycles (Fig. 6a).

Under a confining pressure (σ_3) of 50 kPa, E_0 decreased from 14.24 to 8.82 MPa, and q_t decreased from 202.07 to 157.75 kPa. Under 100 kPa, E_0 declined from 20.09 to 13.00 MPa, and q_t declined from 343.24 to 279.93 kPa. Under 200 kPa, E_0 dropped from 36.12 to 26.62 MPa, and q_t decreased from 674.24 to 603.58 kPa. In addition, the cohesion (c) sharply declined from 10.83 to 6.50 kPa. The internal friction angle (φ) initially decreased and fluctuated, generally between 35° and 40°. This fluctuating (Fan et al., 2024; Jiang TT et al., 2024; Qiu et al., 2024), decreasing trend indicates that the F-T cycle affects not only the bonding and cementation between particles but also the frictional resistance and interlocking behavior of the soil skeleton.

Specifically, in the UCT test, K_1 reached 47.91%, and K_2 reached 38.55%. At 50 kPa, K_1 declined to 38.03%, and K_2 declined to 21.94%. At 100 kPa, K_1 declined to 35.38%, and K_2 declined to 18.44%. At 200 kPa, K_1 was reduced to 26.31%, and K_2 was reduced to 10.48% (Fig. 6b).

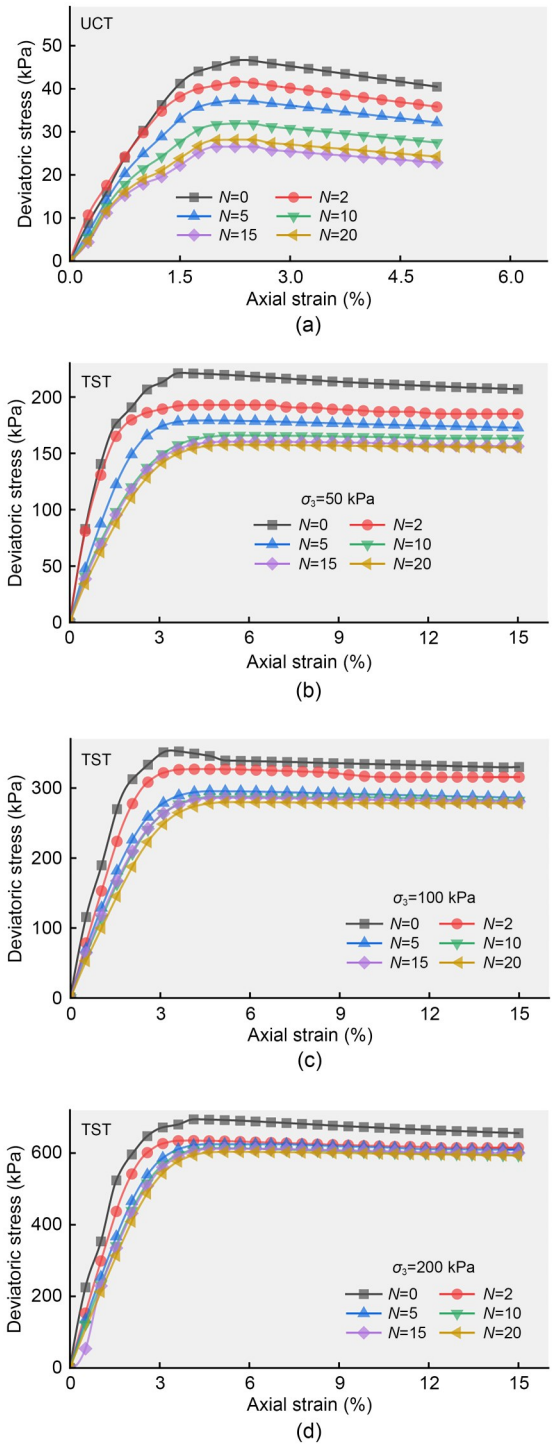


Fig. 5 Stress–strain curves: (a) UCT results; (b) TST results under 50 kPa; (c) TST results under 100 kPa; (d) TST results under 200 kPa

4.3 Application of the new gray model

The predictive performance of the new gray model was evaluated under different confining pressures and

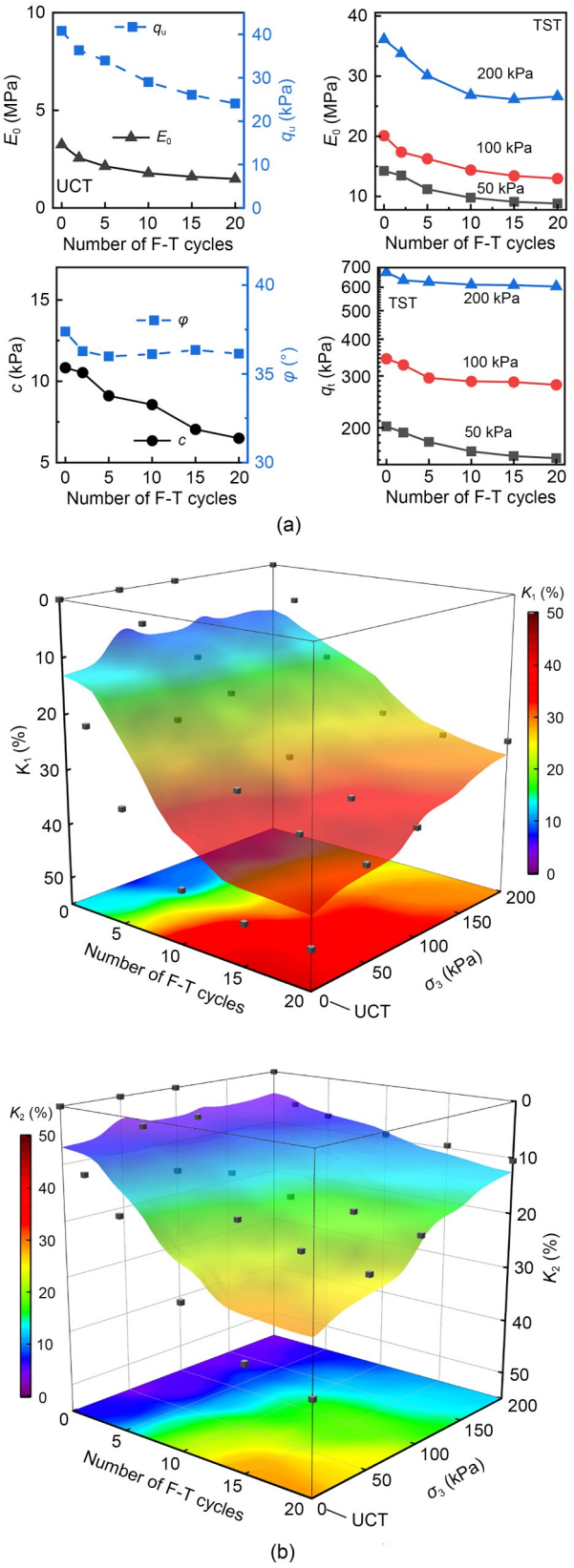


Fig. 6 F-T cycle mechanical deterioration: (a) strength reduction; (b) F-T cycle deterioration rate, K_1 and K_2

F-T cycles (Fig. 7a, Table 2, and Table 3). Overall, the model consistently captures the attenuation trend of mechanical parameters with increasing F-T cycles (R^2> 0.96). At confining pressures of 50, 100, and 200 kPa, the prediction lines exhibit good agreement with the best-fit experimental data (relative error from −4.85% to 3.64%), particularly in describing the early and middle stages in F-T cycles. This observation confirms that the new gray model approach is suitable for characterizing the nonlinear decay process of moraine soil strength parameters.

A similar trend is observed for q_u. The fitted curves reveal a pronounced reduction during the early stage of F-T cycles, followed by a transitional stage of moderate attenuation (middle stage) and finally a plateau stage where the values stabilize (end stage). The prediction curves successfully reproduce the degradation rate and the ultimate strength degradation in the middle-end stage (relative errors of −5.79% to −4.14%). Parameter H represents the ultimate value of the mechanical parameter degradation under F-T cycles. The predicted values (q_t, q_u, and E_0) at N=15 and N=20 showed errors of less than 6%, indicating the good predictive accuracy of the proposed model (Table 3).

Comparison with previous studies further underscores the model's robustness. As shown in Fig. 7b, the predicted results are comparable to those reported by Jiang Y et al. (2024) and Qiu et al. (2023). In particular, the ultimate value (H) aligns closely with the literature, suggesting that the model can be applied across various soil types and testing conditions. In (Jiang Y et al., 2024), types 1, 2, and 3 correspond to moraine soils with dry densities of 2.0, 1.9, and 1.8 g/cm^3, respectively, under a confining pressure of 200 kPa (consolidated drained (CD) test). In (Qiu et al., 2023), types 2 and 3 represent the UCT results of remolded moraine soil with gravel contents of 41.9% and 53.9%, respectively.

This study has several limitations. The experimental tests were conducted with up to 20 F-T cycles, which is sufficient to capture the maximum degradation trends but may not fully reflect the long-term behavior of the soil.

The new gray model was used to predict mechanical properties beyond 20 cycles, but these predictions are extrapolated and have not been directly validated through long-term testing. The study focused on

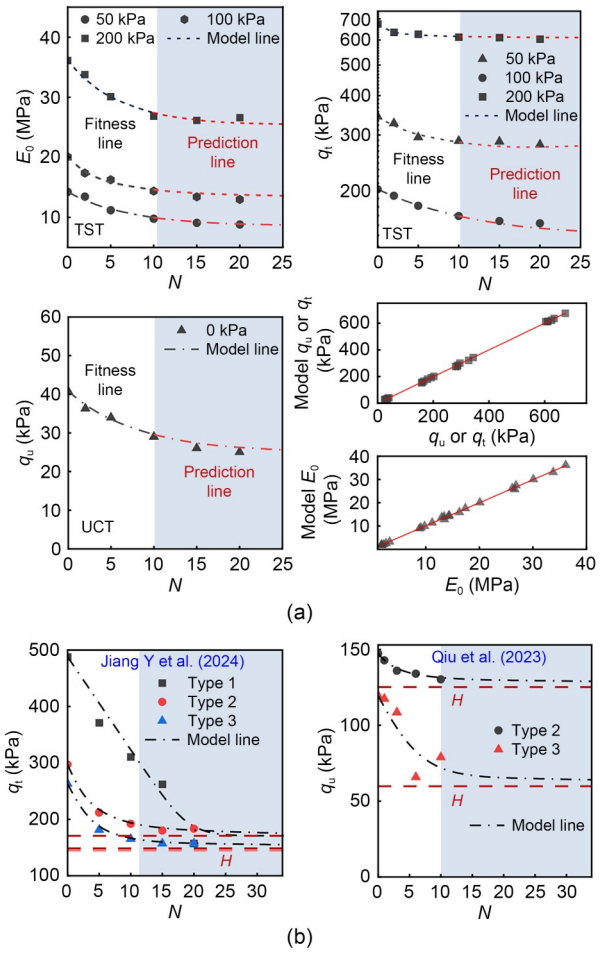


Fig. 7 New gray model prediction: (a) fitness and prediction results; (b) application using data from Jiang Y et al. (2024) and Qiu et al. (2023) (N→+∞)

remolded moraine soil from a specific region, and the findings may not be directly applicable to other soil types or regions.

4.4 Microstructural deterioration

Fig. 8a shows the pore size (>10 μm) range captured by micro-CT and MIP. This indicates that micro-CT can detect approximately half of the total porosity: the MIP-measured porosity is 28.95%. In contrast, micro-CT detects only 14.96% (the porosity of the representative sub-specimen). This limitation arises from the resolution setting of the micro-CT scan (one voxel is 8.0 μm in this study). The 3D pore-crack structure of moraine soils undergoes significant changes over time due to the influence of F-T cycles (Fig. 8b). The microporosity exhibits a rapid initial increase after five cycles. During the initial stage (from zero to five cycles), the microporosity of SS1 ranged from 14.25% to 16.46%, reflecting an increase of approximately 15% to 50%. The average pore size of SS1 increased from 69.83 to 80.58 μm, reflecting an increase of approximately 15% to 30%. This accelerating growth trend slowed in the subsequent cycles (10–20 cycles), with the microporosity of SS1 ranging from 17.33% to 18.69%. The average pore size of SS1 increased from 80.58 to 90.44 μm. The porosity increased from 14.25% to 18.69%, representing a 31% increase.

The F-T cycles significantly affect the shear strength and mechanical properties of moraine soils. One

Table 2 Fitness and prediction of E_0 results using the new gray model

σ_3 (kPa)	λ_1	λ_2	H (kPa)	R^2	K_1^* (%)	E_0 (MPa) (N=15)		Error (%)	E_0 (MPa) (N=20)		Error (%)
						Fitness	Prediction		Fitness	Prediction	
0	−0.29	1.01	1.78	0.99	45	1.70	1.80	−5.61	1.69	1.79	−5.79
50	−0.13	1.01	8.54	0.96	40	9.11	9.26	−1.68	8.82	8.91	−0.95
100	0.00	1.58	13.06	0.98	35	13.42	14.05	−4.85	12.98	13.76	−2.15
200	−0.15	1.01	25.29	0.98	30	26.16	26.23	−0.27	26.62	25.71	3.41

Table 3 Fitness and prediction of strength (q_t or q_u) results using the new gray model

σ_3 (kPa)	λ_1	λ_2	H (kPa)	R^2	K_2^* (%)	q_t or q_u (kPa) (N=15)		Error (%)	q_t or q_u (kPa) (N=20)		Error (%)
						Fitness	Prediction		Fitness	Prediction	
0	−0.10	1.10	24.48	0.98	40	26.05	27.24	−4.57	25.08	26.11	−4.14
50	−0.07	1.07	141.45	1.00	30	160.31	157.49	1.76	157.75	152.01	3.64
100	−0.18	1.01	274.59	0.97	20	285.94	276.19	3.41	279.93	274.85	1.82
200	−0.01	1.91	606.82	0.99	10	610.10	612.28	−0.36	603.58	610.92	−1.22

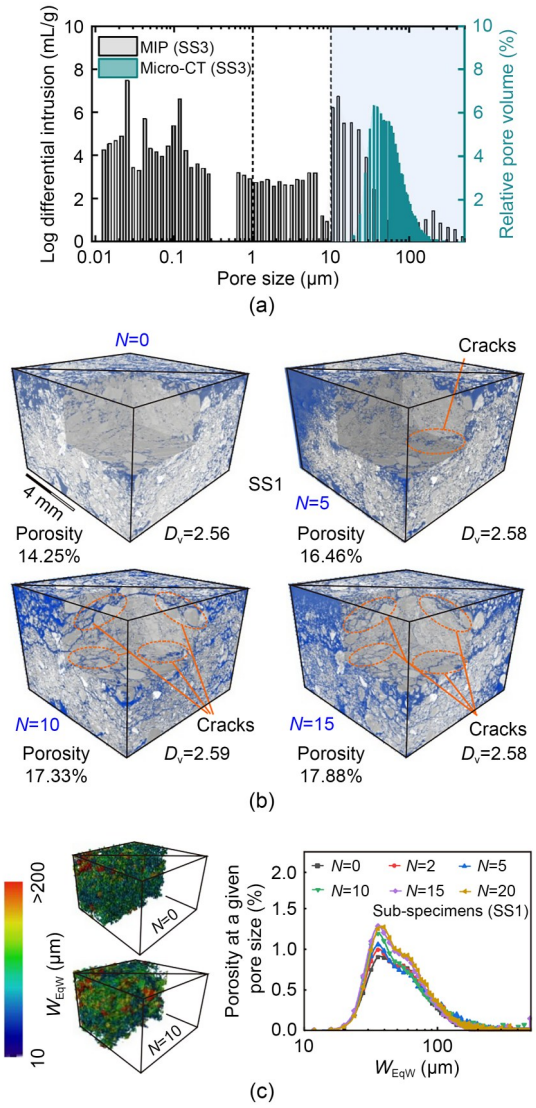


Fig. 8 Pore-crack evolution: (a) MIP vs. micro-CT results; (b) porosity; (c) pore-crack size evolution

important aspect that is closely related to soil behavior under F-T conditions is the formation of shear bands. These localized zones of intense deformation play a crucial role in the mechanical degradation of soils during cyclic F-T processes (Wei et al., 2026). Shear bands not only influence the soil strength but also contribute to the localization of deformation, which in turn accelerates soil degradation. These findings are consistent with the results of this study, where we observed that the mechanical degradation in moraine soils was largely controlled by the development of shear bands, which were observed to form progressively with increasing F-T cycles. The role of shear bands in the mechanical degradation mechanism of soil is critical to understanding how F-T cycles affect the long-term stability of moraine soils in real-world conditions.

5 Conclusions

The mechanical degradation of remolded moraine soils subjected to different F-T cycles was comprehensively investigated in this study, including F-T cycle tests, TSTs, UCTs, and micro-CT scanning. Based on the results, the new gray model was developed to evaluate the mechanical degradation under F-T cycles. Key conclusions are summarized below:

(1) Three distinct stages of mechanical degradation. The mechanical strength of remolded moraine soils decreases significantly with increasing F-T cycles, showing three distinct stages: rapid decline, moderate reduction, and plateau, with parameters such as the initial average elastic modulus (E_0) and shear strength (q_t and q_u) following this three-stage degradation trend. Under a confining pressure of 0–50 kPa, the initial average elastic modulus and strength decrease by 40%–50%, whereas at 100–200 kPa, the decrease is less severe (10%–30%). Higher confining pressures help mitigate deterioration, likely due to partial crack closure.

(2) Key role of microstructural changes. F-T cycles induce significant microstructural changes, primarily the initiation and propagation of pore-crack networks, leading to a 31% increase in porosity. The pore size distribution shifts to larger sizes, with the average equivalent width (W_{EqW}) increasing from 69.83 to 90.44 μm and the microporosity increasing from 14.25% to 18.69%. These microstructural changes are critical in driving the observed mechanical degradation, as they coarsen the soil structure, reduce shear strength, and increase plastic deformation. At the shallow scale, F-T cycles accelerate microstructural deterioration, promoting preferential flow and further reducing shear strength, which makes the soil more prone to localized collapse under heavy rainfall.

(3) The contribution of the new gray model. The newly developed gray model effectively captures the nonlinear deterioration of mechanical parameters, such as strength and elastic modulus, under F-T cycles. By calibrating experimental data from zero to 10 F-T cycles, the model shows high predictive accuracy, with relative errors for strength predictions at the 15th and

20th cycles remaining below 6%. The new gray model not only fits the data from this study but has also been successfully applied to other studies, demonstrating its broad applicability. Importantly, the model's ability to quantify strength degradation provides a reliable estimate of the long-term stability threshold for moraine slopes and infrastructure.

Acknowledgments

This work is supported by the National Natural Science Foundation of China (No. U2544221), the Key Research and Development Program of the Xizang Autonomous Region (No. XZ202401ZY0029), and the Key Program of Natural Science Foundation of the Xizang Autonomous Region (No. XZ202401ZR0073), China.

Author contributions

Tuo LU: methodology, conceptualization, investigation, programming, analysis, and writing–original draft. Yongbo TIE: supervision, conceptualization, writing–review & editing, and funding acquisition. Sai K. VANAPALLI: supervision, conceptualization, methodology, and writing–review & editing. Zhaoyu LI: investigation, analysis, data curation, and visualization.

Conflict of interest

Tuo LU, Yongbo TIE, Sai K. VANAPALLI, and Zhaoyu LI declare that they have no known competing financial interests or personal relationships that could have appeared to influence the work reported in this paper.

Declaration on the use of generative AI tools

During the preparation of this work, the authors used ChatGPT to check grammar and refine academic language of some sentences. After using this tool, the authors reviewed and edited the content as needed and take full responsibility for the content of the publication.

Data availability

Data will be made available on request. The MATLAB code is shown in https://github.com/LuTuo123/LGM.

References

Allen SK, Sattar A, King O, et al., 2022. Glacial lake outburst flood hazard under current and future conditions: worst-case scenarios in a transboundary Himalayan basin. *Natural Hazards and Earth System Sciences*, 22(11):3765-3785. https://doi.org/10.5194/nhess-22-3765-2022

Alom MZ, Taha TM, Yakopcic C, et al., 2019. A state-of-the-art survey on deep learning theory and architectures. *Electronics*, 8(3):292. https://doi.org/10.3390/electronics8030292

Chen NS, Wang Z, Tian SF, et al., 2019. Study on debris flow process induced by moraine soil mass failure. *Quaternary Sciences*, 39(5):1235-1245 (in Chinese). https://doi.org/10.11928/j.issn.1001-7410.2019.05.15

Chen ZM, Liu BL, Liu YH, et al., 2024. Surrounding rock pressure in the tunnel portal section through moraine under freeze-thaw action. *Journal of Mountain Science*, 21(7): 2480-2493. https://doi.org/10.1007/s11629-023-8412-z

Cui P, Zou Q, Xiang LZ, et al., 2013. Risk assessment of simultaneous debris flows in mountain townships. *Progress in Physical Geography: Earth and Environment*, 37(4):516-542. https://doi.org/10.1177/0309133313491445

Emmer A, Klimeš J, Hölbling D, et al., 2020. Distinct types of landslides in moraines associated with the post-lia glacier thinning: observations from the Kinzl Glacier, Huascarán, Peru. *Science of the Total Environment*, 739:139997. https://doi.org/10.1016/j.scitotenv.2020.139997

Fan JK, Yue ZR, Han ZH, et al., 2024. Study on prediction model of strength deterioration of moraine soil under high frequency freeze-thaw cycles. *Journal of Glaciology and Geocryology*, 46(2):602-611 (in Chinese). https://doi.org/10.7522/j.issn.1000-0240.2024.0049

Feng JD, Li JG, Wang R, et al., 2008. Large scale direct shear test on strength behavior of railway moraine soils in Yunnan. *Rock and Soil Mechanics*, 29(12):3205-3210 (in Chinese). https://doi.org/10.3969/j.issn.1000-7598.2008.12.005

Han Z, Vanapalli SK, Kutlu ZN, 2016. Modeling behavior of friction pile in compacted glacial till. *International Journal of Geomechanics*, 16(6):D4016009. https://doi.org/10.1061/(ASCE)GM.1943-5622.0000659

Jiang HR, Zheng GH, Yi YH, et al., 2020. Progress and challenges in studying regional permafrost in the Tibetan Plateau using satellite remote sensing and models. *Frontiers in Earth Science*, 8:560403. https://doi.org/10.3389/feart.2020.560403

Jiang TT, Pan HL, Ai YF, et al., 2024. Effect of freeze-thaw cycles and water content on the mechanical properties of moraine soil. *Bulletin of Geological Science and Technology*, 43(2):238-252 (in Chinese). https://doi.org/10.19509/j.cnki.dzkq.tb20220649

Jiang Y, Lu XS, Liu ZM, et al., 2024. Experimental study on the engineering properties and failure mechanism of moraine in southeast Tibet under freeze–thaw cycles conditions. *Engineering Failure Analysis*, 163:108551. https://doi.org/10.1016/j.engfailanal.2024.108551

Li CD, Wang R, Gu DM, et al., 2022. Temperature and ice form effects on mechanical behaviors of ice-richmoraine soil of Tianmo valley nearby the Sichuan-Tibet Railway. *Engineering Geology*, 305:106713. https://doi.org/10.1016/j.enggeo.2022.106713

Li ML, Liu JN, Jiang YJ, et al., 2025. The study of microscopic damage in moraine soils under freeze-thaw cycles based on discrete element. *Bulletin of Engineering Geology and the Environment*, 84(11):558. https://doi.org/10.1007/s10064-025-04606-3

Liu H, Dai XY, Yang GS, et al., 2024. Damage evolution characteristics of freeze–thaw rock combined with CT image and deep learning technology. *Bulletin of Engineering Geology and the Environment*, 84(1):20.

https://doi.org/10.1007/s10064-024-04010-3

Lu T, Tang YM, Tie Y, et al., 2023. Fractal analysis of small-micro pores and estimation of permeability of loess using mercury intrusion porosimetry. *Journal of Zhejiang University-SCIENCE A*, 24(7):584-595. https://doi.org/10.1631/jzus.A2200528

Lu T, Tie Y, Song SY, et al., 2025. Quantitative assessment of calcareous cementation in moraine soils: insights from an integrated mineralogical and granulometric analysis. *Bulletin of Engineering Geology and the Environment*, 84(11): 479. https://doi.org/10.1007/s10064-025-04451-4

Minaee S, Boykov YY, Porikli F, et al., 2022. Image segmentation using deep learning: a survey. *IEEE Transactions on Pattern Analysis and Machine Intelligence*, 44(7):3523-3542. https://doi.org/10.1109/TPAMI.2021.3059968

MOHURD (Ministry of Housing and Urban-Rural Development), SAMR (State Administration for Market Regulation). 2019. Standard for Geotechnical Testing Method, GB/T 50123-2019. National Standards of the People's Republic of China.

Qiu E, He Q, Chen Q, et al., 2023. Influence of freeze–thaw cycles on mechanical properties of moraine soils. *Transportation Geotechnics*, 42:101097. https://doi.org/10.1016/j.trgeo.2023.101097

Qiu EX, Pan HY, He QL, et al., 2024. Experimental investigation and model study on mechanical properties of moraine soils under freeze-thaw cycles. *Journal of Engineering Geology*, 32(3):772-784 (in Chinese). https://doi.org/10.13544/j.cnki.jeg.2023-0351

Rechberger C, Fey C, Zangerl C, 2021. Structural characterisation, internal deformation, and kinematics of an active deep-seated rock slide in a valley glacier retreat area. *Engineering Geology*, 286:106048. https://doi.org/10.1016/j.enggeo.2021.106048

Vanapalli SK, Han Z, 2016. Modelling the mechanical properties of a compacted glacial till. *Indian Geotechnical Journal*, 46(3):261-271. https://doi.org/10.1007/s40098-016-0183-9

Wang Q, Liu J, Li X, et al., 2025. Expansion mechanism of sulfate attack on cement-treated aggregates under freeze–thaw cycles. *Journal of Zhejiang University-SCIENCE A*, 26(1):36-49. https://doi.org/10.1631/jzus.A2300590

Wang R, Li CD, Gu DM, et al., 2024. Strength criterion of ice-rich moraine soil considering the ice form and temperature based on thermal-mechanical triaxial tests. *Cold Regions Science and Technology*, 220:104150. https://doi.org/10.1016/j.coldregions.2024.104150

Wei X, Shen YJ, Wei ZL, et al., 2025. Resistivity and unfrozen water content of moraine soil at freezing temperatures: experiments and thermodynamic modeling. *Cold Regions Science and Technology*, 235:104494. https://doi.org/10.1016/j.coldregions.2025.104494

Wei X, Shen YJ, Wang YZ, et al., 2026. Shear behaviors of freeze–thaw interface in moraine soil: experimental and theoretical approaches. *Journal of Rock Mechanics and Geotechnical Engineering*, in press. https://doi.org/10.1016/j.jrmge.2026.01.012

Wei YN, Fan W, Yu B, et al., 2020. Characterization and evolution of three-dimensional microstructure of malan loess. *CATENA*, 192:104585. https://doi.org/10.1016/j.catena.2020.104585

Winter MG, 2004. Determination of the acceptability of glacial tills for earthworks. *Quarterly Journal of Engineering Geology and Hydrogeology*, 37(3):187-204. https://doi.org/1010.1144/1470-9236/04-017

Wu YP, Guo J, Guo CX, et al., 2010. Exothermic process of cast-in-place pile foundation and its thermal agitation of the frozen ground under a long dry bridge on the Qinghai-Tibet Railway. *Journal of Zhejiang University-SCIENCE A*, 11(2):88-96. https://doi.org/10.1631/jzus.A0900522

Yu B, Dijkstra TA, Fan W, et al., 2024. Advanced multi-scale characterization of loess microstructure: integrating μXCT and FIB-SEM for detailed fabric analysis and geotechnical implications. *Engineering Geology*, 341:107727. https://doi.org/10.1016/j.enggeo.2024.107727

Zeng ZX, Zhang LM, Xu ZD, et al., 2024. Mechanical behaviour and grain breakage characteristics of Tibetan glacial tills under triaxial compression. *Acta Geotechnica*, 19(7): 4809-4822. https://doi.org/10.1007/s11440-023-02195-7

Zhou GGD, Chen LL, Mu QY, et al., 2019. Effects of water content on the shear behavior and critical state of glacial till in Tianmo Gully of Tibet, China. *Journal of Mountain Science*, 16(8):1743-1759. https://doi.org/10.1007/s11629-019-5440-9